

Sea Breeze Theory and Applications

JOHN E. WALSH¹

Dept. of Meteorology, Massachusetts Institute of Technology, Cambridge 02139

(Manuscript received 27 March 1974)

ABSTRACT

The linearized Boussinesq equations with rotation, viscosity, conduction, and a mean stratification are used to model the sea breeze in two dimensions. The motion is forced by a prescribed surface temperature function.

The linear model produces a sea breeze with realistic velocities and spatial dimensions. Hydrostatic solutions are found to differ very little from nonhydrostatic solutions. The only distinguishing feature of the solution at the inertial latitude is an amplitude maximum far from the coastline. Both the phase and the amplitude depend on the mean atmospheric stability. The computed vertical heat fluxes, when summed along the coastlines of the principal land masses, indicate that the sea breeze effect can account for several percent of the globally averaged vertical flux of sensible heat at a height of several hundred meters.

The land-sea temperature difference required by the model to create a net onshore flow in opposition to a basic current agrees well with the empirical criterion defined by Biggs and Graves.

The nonlinear advection process is studied with a finite-difference model based on a series of overlapping grids. The principal effect of the nonlinear terms is a landward advection of the sea breeze circulation.

1. Introduction

The sea breeze is a mesoscale response of the atmosphere to horizontal variations in surface heating. Because it is generally restricted to the lowest 1–2 km, the sea breeze is strongly influenced by the boundary layer processes of viscosity and conduction. Yet its horizontal extent is large enough that the earth's rotation and the synoptic-scale pressure gradient cannot be ignored.

Both analytic and numerical studies of the sea breeze have appeared in the literature. In the former, solutions have been obtained only after simplifying the governing equations to the point where certain physical processes are omitted. Conduction, for example, is omitted by Schmidt (1947), Pierson (1950), and Smith (1955), each of whom specifies the heating as a function of space and time. Diffusion of momentum is neglected by Defant (1951) as well as by Schmidt and Smith. Geisler and Bretherton (1969) also omit viscosity and conduction in their model of the sea breeze "fore-runner." Malkus and Stern (1953), the first to include a basic current, neglect viscous and Coriolis effects in a model of airflow over a heated island. In a recent study of the urban heat island, Olfe and Lee (1971) include a basic current but consider the effects of rotation and viscosity only separately.

Numerical modellers are faced with the problem of adequately resolving the steep temperature and velocity

gradients which are found near the coastline in sea breeze situations. Yet the lateral boundaries must be sufficiently far from the coastline that boundary effects do not contaminate the solution. In order to avoid the excessive storage requirements of a uniform fine grid, some previous investigators (Fisher, 1961; Estoque, 1961; Moroz, 1967) have used stretched coordinate systems, while others have settled for the poorer resolution of a uniform coarse grid in which the horizontal space increment is 4 km (McPherson, 1968; Neumann and Mahrer, 1971) or even 11 km (Pielke, 1973). In each of these models, computational stability was achieved only through the use of such devices as external filters, upstream space differencing, or artificial horizontal diffusion terms.

The cost limitations and the stability problems associated with finite-difference models suggest that the analytic approach may be the most fruitful in a study of the sea breeze. It is the author's opinion that the potential of the analytic model is largely untapped. This paper will therefore develop an analytic model and will use finite-differencing techniques only to test several assumptions which are made in applying the analytic results. With the exception of nonlinear advection, all the relevant forces are included in the analytic model of Section 2. However, the formulation is kept relatively simple so that we may obtain solutions easily and examine the model's properties thoroughly. For example, the eddy diffusion coefficients are assumed to be constant in space and time rather than functions of the Richardson number as in Estoque's model. In

¹ Present affiliation: Laboratory for Atmospheric Research, Urbana, Ill.

view of the large uncertainties in current estimates of eddy diffusivities (especially horizontal diffusivities), one coefficient is used to represent both horizontal and vertical diffusion of momentum and buoyancy. An examination of the model results in Section 3 shows that the model produces a realistic sea breeze despite the simplified treatment of diffusion. The results can then be used in a variety of applications, among which is a study of the role played by the sea breeze in the general circulation.

The scaling of the velocity components is such that one can determine the land-sea temperature difference required to create a net onshore flow in the presence of an offshore gradient wind. Such a relationship is of practical value in forecasting the occurrence of a sea breeze but has never been derived theoretically. The theoretical criterion is found in Section 5 to agree well with empirical criteria, although construction of the theoretical criterion requires that the effects of nonlinear advection be anticipated. The assumptions concerning nonlinear advection are supported by the nonlinear computations described in Section 6. The nonlinear results are also of some technical interest because they are based on an overlapping grid network rather than on the coordinate stretching techniques used in earlier models.

2. Formulation of the linear model

The model will employ the Cartesian geometry sketched in Fig. 1. The x axis is oriented perpendicular to the coastline. All variables are assumed to be uniform in the y direction. Uniform rotation about the z axis is assumed.

Because the sea breeze rarely extends to heights > 1-2 km, the Boussinesq equations are used. Rotation, viscosity and conduction are included. When linearized about a basic current U normal to the coastline, these equations are

$$\frac{\partial u}{\partial t} + U \frac{\partial u}{\partial x} - fv = -\frac{\partial p}{\partial x} + \nu \nabla^2 u, \tag{1}$$

$$\frac{\partial v}{\partial t} + U \frac{\partial v}{\partial x} + fu = \nu \nabla^2 v, \tag{2}$$

$$\frac{\partial w}{\partial t} + U \frac{\partial w}{\partial x} = -\frac{\partial p}{\partial z} + b + \nu \nabla^2 w, \tag{3}$$

$$\frac{\partial b}{\partial t} + U \frac{\partial b}{\partial x} + N^2 w = \kappa \nabla^2 b, \tag{4}$$

$$\frac{\partial u}{\partial x} + \frac{\partial w}{\partial z} = 0, \tag{5}$$

where $\nabla^2 = \partial^2/\partial x^2 + \partial^2/\partial z^2$, $p = (p - p_a)/\rho_a$, $b = g(T - T_0 + g c_p^{-1} z)/T_0$, $N^2 = db/dz$, c_p is the specific heat of dry

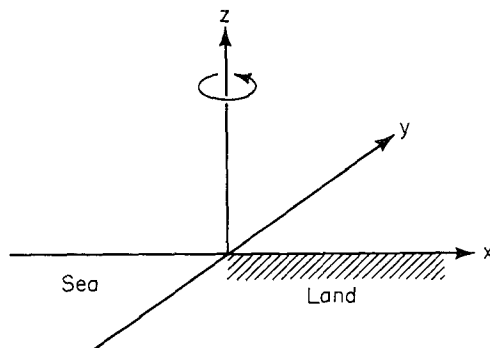


FIG. 1. Geometry of the linear model.

air, and the subscripts 0 and a refer to the surface and an adiabatic atmosphere, respectively. The variables (u, v, w) are the velocity components in (x, y, z) directions. The "buoyancy" b and the "pressure" p represent the deviations of temperature and pressure, respectively, from the temperature and pressure in an adiabatic atmosphere (Ogura and Phillips, 1962). The Brunt-Väisälä frequency N^2 , a stability index, gives the increase with height of the horizontally averaged buoyancy; ν and κ are the eddy coefficients of viscosity and conduction. The Coriolis parameter is $f = 2\omega \sin\phi$ where $\omega = (2\pi/24)$ hr⁻¹ and ϕ is the latitude. Constant values are assigned to f , N^2 , U , ν , and κ ($\nu = \kappa$). For later reference, we note that the hydrostatic approximation can be made in (1)-(5) by neglecting $\partial^2/\partial x^2$ in the Laplacian operators and by retaining only the pressure and buoyancy terms in (3).

The boundary conditions are that all variables remain finite at large z , that u , v and w vanish at the ground, and that b reduce to the specified forcing function at $z=0$. This forcing function varies periodically with time to simulate the diurnal cycle:

$$b = \begin{cases} b_{\max} \sin\omega t, & x > 0 \\ 0 & x = 0 \\ -b_{\max} \sin\omega t, & x < 0 \end{cases} \tag{6}$$

where b_{\max} is a positive real constant. The time $t=0$ corresponds to sunrise. The inclusion of only the first harmonic in (6) is an idealization since observed surface temperature curves are not perfect sinusoids. Fourier analysis of Lettau's (1949, 1951) data for typical inland stations indicates that the second harmonic contains 6-12% as much of the surface temperature variation as the first harmonic contains.

Time is scaled by the forcing frequency ω , buoyancy by the amplitude b_{\max} of the surface buoyancy perturbation in (6), and both horizontal and vertical distances by the diffusive length $L = (\kappa/\omega)^{1/2}$. For the typical value of $\kappa = 5 \times 10^4$ cm² sec⁻¹, L is approximately 250 m. Denoting nondimensional variables by primes, the com-

plete scaling is

$$\begin{aligned}
 L &= (\kappa/\omega)^{\frac{1}{2}} \\
 U &= \omega L U_{nd} \\
 t &= \omega^{-1} t' & b &= b_{\max} b' \\
 (x, z) &= L(x', z') & (u, v, w) &= b_{\max} \omega^{-1} (u', v', w') \\
 \frac{\partial}{\partial t} - \nu \nabla^2 &= \omega \left(\frac{\partial}{\partial t'} - \nabla'^2 \right) & p &= b_{\max} L p'.
 \end{aligned}$$

We note that the dimensional velocities are directly proportional to the maximum land-sea temperature difference. Dropping the primes, introducing the streamfunction ψ ($u = -\partial\psi/\partial z$, $w = \partial\psi/\partial x$), and substituting the nondimensional variables into (1)-(5), one obtains a set of four equations involving the unknowns ψ , v , p , b and the three external parameters f/ω , N^2/ω^2 , $U(\omega L)^{-1}$. The value of $\nu = \kappa$ enters the solution only by determining the length scale L and the strength of the basic current.

Solutions are obtained by using Fourier integrals for the x dependence:

$$(\psi, v, p, b) = \text{Re} \left[\int_{-\infty}^{\infty} (\Psi, V, P, B) e^{i(kx+zt)} dk \right], \quad (7)$$

where Ψ , V , P , B are functions of k and z . The equations for Ψ and B are

$$\left[\left(\mathcal{L}^2 + \frac{f^2}{\omega^2} \right) \frac{\partial^2}{\partial z^2} - \left(\mathcal{L}^2 + \frac{N^2}{\omega^2} \right) k^2 \right] \Psi = 0, \quad (8)$$

$$\mathcal{L} \left[\left(\mathcal{L}^2 + \frac{f^2}{\omega^2} \right) \frac{\partial^2}{\partial z^2} - \left(\mathcal{L}^2 + \frac{N^2}{\omega^2} \right) k^2 \right] B = 0, \quad (9)$$

where

$$\begin{aligned}
 \mathcal{L} &\equiv \mu^2 - \frac{\partial^2}{\partial z^2}, \\
 \mu &\equiv [i(1 + U_{nd}k) + k^2]^{\frac{1}{2}}, \quad \text{Re}\{\mu\} \geq 0.
 \end{aligned}$$

The solution for which $\Psi=0$ and $\mathcal{L}B=0$ is a hydrostatic, geostrophic solution ($\partial\Psi/\partial x = \partial\Psi/\partial z = 0$) in which the vertical structure is such that time changes in V and B are due solely to viscosity and conduction.

Substituting solutions of the form $e^{-\lambda z}$ into (8) or (9) gives a characteristic equation in λ :

$$\left[(\lambda^2 - \mu^2)^2 + \frac{f^2}{\omega^2} \right] \lambda^2 - k^2 \left[(\lambda^2 - \mu^2)^2 + \frac{N^2}{\omega^2} \right] = 0. \quad (10)$$

The roots in λ , which are complex and occur in three pairs of the form $\pm(a+bi)$, are obtained numerically from (10). The upper boundary conditions require that only roots with positive real parts be chosen; these are

denoted by $\lambda_2, \lambda_3, \lambda_4$, while $\mu \equiv \lambda_1$. The vertical dependence can then be written as

$$\left. \begin{aligned}
 \Psi(k, z) &= \sum_{j=2}^4 \psi_j e^{-\lambda_j z} \\
 B(k, z) &= b_1 e^{-\mu z} + \sum_{j=2}^4 \alpha_j \psi_j e^{-\lambda_j z} \\
 V(k, z) &= -ik\omega(\mu f)^{-1} b_1 e^{-\mu z} + \sum_{j=2}^4 \gamma_j \psi_j e^{-\lambda_j z} \\
 P(k, z) &= -\mu^{-1} b_1 e^{-\mu z} + \sum_{j=2}^4 \epsilon_j \psi_j e^{-\lambda_j z}
 \end{aligned} \right\}$$

where $b_1, \psi_2, \psi_3, \psi_4$ are constant coefficients, and

$$\left. \begin{aligned}
 \alpha_j &= ikN^2\omega^{-2}(\lambda_j^2 - \mu^2)^{-2}, & j &= 2, 3, 4 \\
 \gamma_j &= f\lambda_j\omega^{-1}(\lambda_j^2 - \mu^2)^{-2}, & j &= 2, 3, 4 \\
 \epsilon_j &= ik\lambda_j^{-1}(\mu^2 - \lambda_j^2) - \alpha_j\lambda_j^{-1}, & j &= 2, 3, 4
 \end{aligned} \right\}.$$

The surface boundary conditions on u, v, w and b become

$$\left. \begin{aligned}
 \sum_{j=2}^4 \lambda_j \psi_j &= 0 \\
 -ik\omega(\mu f)^{-1} b_1 + \sum_{j=2}^4 \gamma_j \psi_j &= 0 \\
 \sum_{j=2}^4 \psi_j &= 0 \\
 b_1 + \sum_{j=2}^4 \alpha_j \psi_j &= -\frac{1}{\pi k}
 \end{aligned} \right\}. \quad (11)$$

Eq. (11) is a system of four simultaneous linear equations which can be solved for $b_1, \psi_2, \psi_3, \psi_4$ to complete the solution for a single wave component. The problem is then reduced to an integration over k for fixed x, z, t according to the previous definitions of the Fourier integrals.

3. Results of the linear model

a. Results with no basic current

Before the computed circulations are examined, the effect of the hydrostatic approximation will be noted. Neumann and Mahrer (1971) claim that the vertical acceleration $\partial w/\partial t$ cannot be neglected. However, their scale analysis is based on an adiabatic stratification and the *a priori* assumption that the pressure variation has a magnitude ρW^2 . In a more consistent approach, the horizontal equation of motion is used to scale the pressure variation. Denoting the horizontal and vertical length scales by L_x and L_z , the velocity scales by U and W ($U/L_x \sim W/L_z$), and the time scale by τ , one obtains

$$\left. \begin{aligned}
 \delta p &\sim L\rho U\tau^{-1} \\
 \frac{1}{\rho} \frac{\partial p}{\partial z} &\sim \frac{L_x^2 W}{L_z^2 \tau} \sim \frac{L_x^2}{L_z^2} \frac{\partial w}{\partial t}
 \end{aligned} \right\}.$$

TABLE 1. Values of u, v, w (cm sec⁻¹) at $t=6$ hr for the case of $U=0, f/\omega=1.5, N^2=10^{-4}$ sec⁻², $b_{\max}=9.8$ cm sec⁻². The headings "hyd" and "non" indicate hydrostatic and nonhydrostatic solutions, respectively. The coordinates x and z are nondimensional.

		$x=1.0$		$x=5.0$		$x=25.0$		$x=105.0$	
		hyd	non	hyd	non	hyd	non	hyd	non
$z=4$	u	-24.1	-24.1	-24.1	-24.1	-25.5	-25.6	-6.99	-6.99
	v	-34.8	-34.1	-31.2	-31.4	-22.1	-22.1	-18.1	-18.1
	w	0.00	0.00	0.00	0.00	-0.07	-0.07	0.29	0.29
$z=2$	u	-78.9	-78.9	-82.4	-82.3	-14.0	-14.0	29.9	29.9
	v	41.5	42.5	36.2	35.9	11.8	11.8	18.9	18.9
	w	0.01	0.04	-0.55	-0.53	1.95	1.95	0.74	0.74
$z=1$	u	13.5	16.7	114.	114.	120.	120.	30.7	30.7
	v	-6.26	-5.55	-28.0	-27.9	-23.2	-23.2	22.1	22.1
	w	0.35	1.17	8.65	8.59	2.89	2.89	0.39	0.39
$z=\frac{2}{3}$	u	202.	201.	251.	251.	138.	138.	25.2	25.2
	v	-39.7	-38.6	-50.4	-50.2	-26.9	-26.9	16.7	16.7
	w	20.0	18.8	10.0	10.0	1.91	1.91	0.22	0.22
$z=\frac{1}{3}$	u	413.	411.	266.	266.	106.	106.	15.7	15.7
	v	-47.1	-46.2	-42.2	-42.2	-18.7	-18.7	8.91	8.91
	w	27.2	27.1	4.94	4.99	0.67	0.67	0.07	0.07

Any *a priori* conclusion about hydrostatic balance depends then on a knowledge of L_x/L_z , a ratio which is not determined by the usual formulation of the sea breeze problem. However, it is inconsistent to use a horizontal grid increment of 4 km and a total depth of 2 km, as Neumann and Mahrer did, if nonhydrostatic effects are thought to be significant. Pielke (1972) found that the ratio of the horizontal and vertical space increments can determine the validity of the hydrostatic approximation in a numerical model, since his hydrostatic and nonhydrostatic results diverged only for small values of $\Delta x/\Delta z$.

Table 1 shows the hydrostatic and nonhydrostatic velocities at $t=6$ hr computed from the linear equations for the case of $U=0, f/\omega=1.5$ ($\phi=48.6^\circ$), and $N^2=10^{-4}$ sec⁻². Since there is no basic current, the circulation is symmetric about the coastline. The velocities are dimensionalized by assuming that $b_{\max}=9.8$ cm sec⁻², corresponding to a maximum land-sea temperature difference of about 5.5C. The results in Table 1, which are free from the computational problems of Pielke's (1972) study, show that the hydrostatic approximation does not change the linear results significantly. It is therefore of little consequence that the remainder of the results in Sections 3, 4 and 5 are obtained from the nonhydrostatic formulation (1)-(5).

Fig. 2 shows the computed horizontal wind vectors at the coastline for five levels in the vertical. Again, $U=0, f/\omega=1.5$, and $N^2=10^{-4}$ sec⁻². Vectors are plotted at 2-hr intervals beginning at $t=0$ (sunrise), at which time the remnants of the land breeze are still present. An onshore sea breeze flow develops near the surface by $t=2$ hr and reaches a depth of several hundred meters later in the day. The increase with time of the depth of the onshore flow is consistent with the observations of Fisher (1960). On the other hand, the model of Geisler and Bretherton (1969) predicts a disturbance which settles to the ground as time progresses.

The difference is presumably due to the fact that Geisler and Bretherton introduced the differential heating instantaneously, while in the present model the buoyancy accelerates the circulation continuously and is periodic in time.

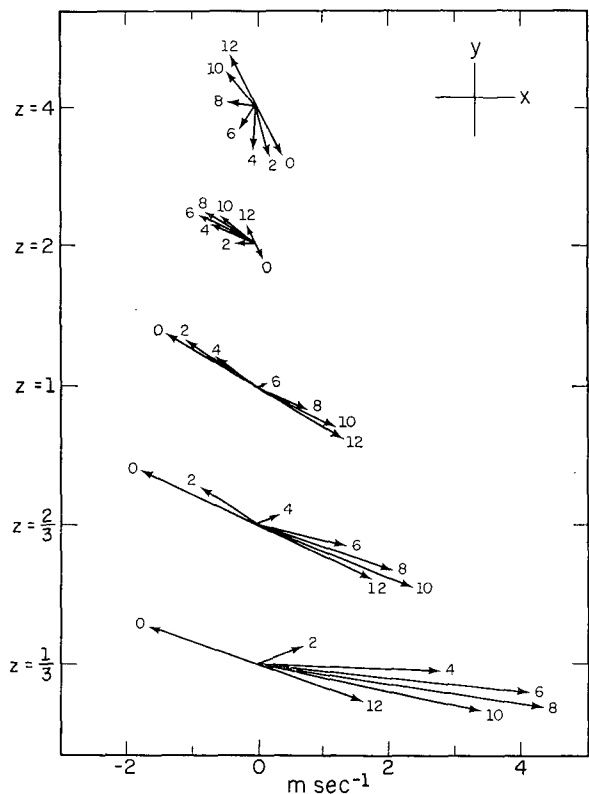


FIG. 2. Horizontal wind vectors at $x=0$ for the case of $f/\omega=1.5, N^2=10^{-4}$ sec⁻², $U=0$. Velocities (m sec⁻¹) are scaled using $b_{\max}=9.8$ cm sec⁻² and are plotted at 2-hr intervals. The height z is nondimensional.

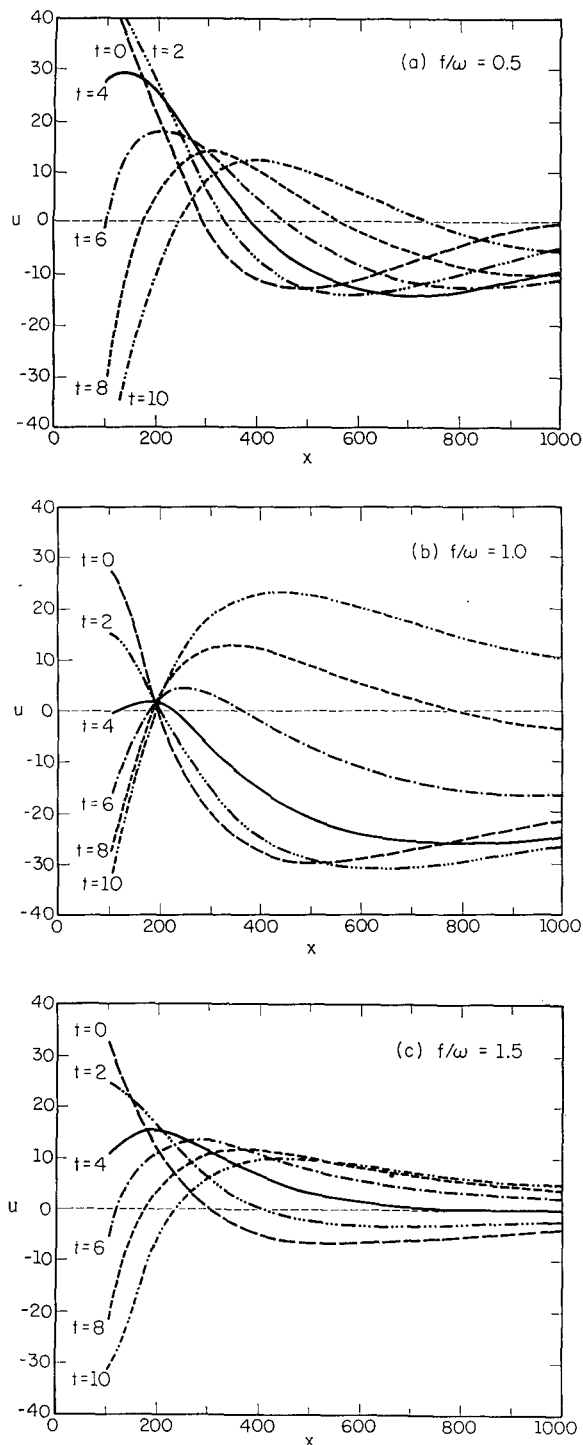


FIG. 3. Variation of the u component of the velocity with x at $z=4$ for the case of $U=0$, $N^2=10^{-4} \text{ sec}^{-2}$, and (a) $f/\omega=0.5$, (b) $f/\omega=1.0$, (c) $f/\omega=1.5$. The distance x is nondimensional, t is in hours. Velocities (cm sec^{-1}) are scaled using $b_{\text{max}}=9.8 \text{ cm sec}^{-2}$.

In the upper-level return current, maximum wind speeds are less than 50% as strong as those in the low-level flow. As required by mass continuity, the

layer of significant ($\gtrsim 20 \text{ cm sec}^{-1}$) offshore winds is 2-3 times deeper at $x=0$ than the layer of onshore winds.

According to Table 1, the wind speeds near the surface decrease rapidly with distance from the coastline. At higher levels, the decrease is slower. The x dependence of the computed buoyancies was similar: b was found to differ by less than 5% from the diffusive solution

$$b_{\text{diff}} = b_0 \exp(2^{-1/2}z) \sin(t - 2^{-1/2}z),$$

for all $x \geq 100$ at $z = \frac{1}{3}$ and for all $x \geq 500$ at $z = 4$. The model therefore predicts a sea breeze "influence region" inside which the N^2w effect is an important contributor to the time changes in b .

The very large values of $|\partial(u,v,w)/\partial x|$ near the surface are evidently due to the absence of temperature advection. In the atmosphere, the advection of cooler temperatures from offshore will tend to reduce the temperature of the land near the coastline. As a result of the "smoothed" forcing function, the motion will be less concentrated near $x=0$ than it is in the model. The smoothing of the surface temperature field can be included in the model either by removing the discontinuity in the forcing function or by including a nonzero basic current. The results of the latter approach are discussed in the next section.

The dependence of the circulation on f was examined by comparing solutions in which the Coriolis frequency is less than ($f/\omega=0.5$), equal to ($f/\omega=1.0$), and greater than ($f/\omega=1.5$) the forcing frequency ω . The corresponding latitudes are 14.5, 30.0 and 48.6N. At $x=0$, the wind vectors for the two lower latitudes differ very little from those in Fig. 2. The winds rotate in the expected clockwise sense at all z under the influence of Coriolis deflection. At large x and z , however, the f dependence is very noticeable. As shown in Fig. 3, a

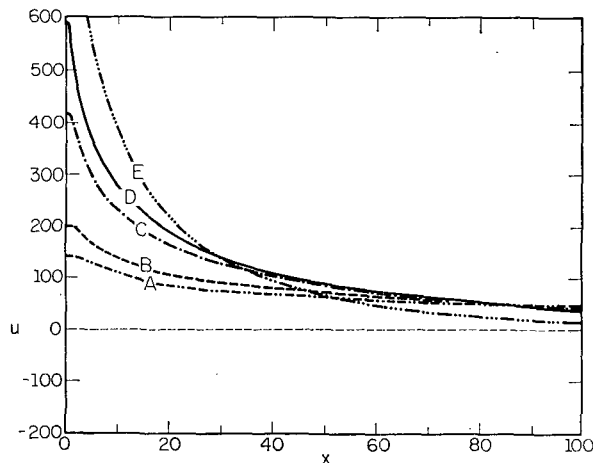


FIG. 4. The x dependence of the u component of the velocity at $z=0.33$, $t=8 \text{ hr}$ for the case of $f/\omega=1.5$, $U=0$. Results are shown for five values of N^2 (sec^{-2}): (A) 10^{-3} , (B) 5×10^{-4} , (C) 10^{-4} , (D) 5×10^{-5} , (E) 10^{-5} . Otherwise as in legend to Fig. 3.

standing wave develops in the u field at the inertial latitude ($f/\omega=1.0$), and the amplitude of the disturbance is considerably larger at the inertial latitude than at the higher and lower latitudes. This behavior becomes extreme in the limiting case of no viscosity and conduction where, if the forcing is of the form $w_0 \sim \cos kx \sin \omega t$, the u solution is undefined at the inertial latitude. When included in the equations, viscosity evidently limits the magnitude of u and masks any resonance-like behavior. Only at large x and z , where frictional effects are reduced, is the $f=\omega$ amplitude maximum apparent.

The effect of the stability on the low-level flow is illustrated in Fig. 4, which shows $u(x)$ at $z=\frac{1}{3}$ when the horizontal winds are well developed, $t=8$ hr. Curves are sketched for five values of N^2 . Near the coastline, the winds are strongest when the stability is weakest. This suggests that the observed weakness of the land breeze may be attributed to the higher nighttime stability of the atmosphere. The larger magnitudes of $\partial u/\partial x$ when N^2 is small are associated with larger values of w , as required by the continuity equation. Physically, a nearly unstable stratification ($N^2=10^{-5}$ sec $^{-2}$) offers little resistance to motion in the vicinity of the temperature discontinuity, so most of the potential energy is released near $x=0$. When the stratification is very stable, w , $|\partial w/\partial z|$ and $|\partial u/\partial x|$ are small, and the winds weaken less rapidly with distance from the coastline. This tendency for a stable atmosphere to be inelastic results in a more rapid inland propagation of the disturbance when N^2 is large. Fig. 5 shows the sea breeze onset time, at which u changes from negative to positive, as a function of N^2 . The earlier onset time when the stratification is stable is evident at all inland points. The inland extent of the sea breeze, defined as the value of x at which $u=0$ for fixed z and t , can therefore be said to increase with increasing N^2 . This result suggests an analogy between the circulation's horizontal extent and the Rossby deformation radius NH/f , where H is the depth of the disturbance.

Observational verification of the dependence of N^2 requires both upper air and hourly surface data for a representative number of sea breeze days at a given location. In a synoptic study of sea breeze occurrences during 1970-72, the author found no significant correlation between the sea breeze onset time (hours after sunrise) and the surface-to-850 mb stability at Portland, Me. However, at Charleston, S. C., a significant negative correlation supported the model results. It is difficult to base any conclusions on this type of study because the effect of the gradient wind may contribute to an apparent dependence of the onset time on the stability. The most stable stratifications (inversions) are generally found when the gradient wind is calm, and calm conditions favor rapid sea breeze development.

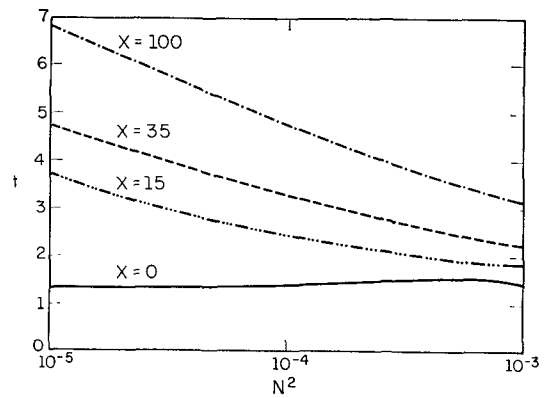


FIG. 5. Sea breeze onset time (hours after sunrise) for the case of $f/\omega=1.5$, $U=0$. Results are shown for four nondimensional values of x ; all curves are for $z=0.33$.

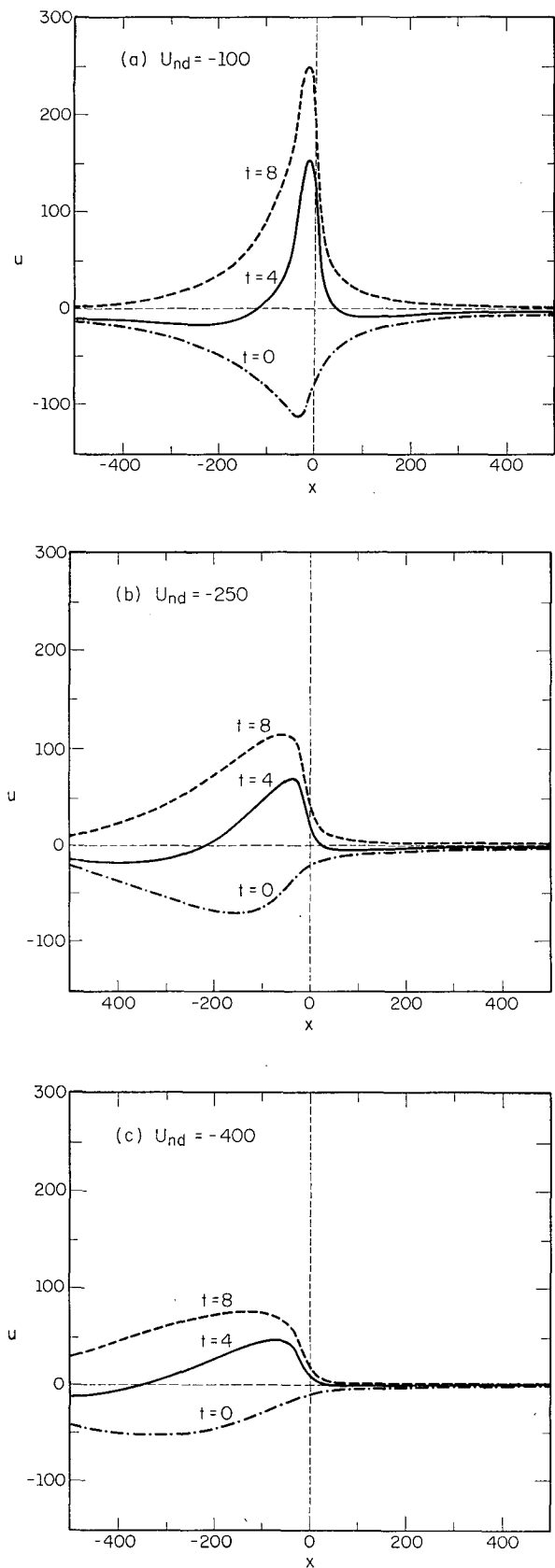
b. Results with a basic current

Because of its role in advecting the perturbation quantities, the gradient wind U cannot be neglected in a study of the sea breeze. It was seen in Section 3a that the velocity gradients near the coastline are very steep when $U=0$ in the linear formulation.

Results were computed for the following values of the nondimensional basic current: $U_{nd} = -50, -100, -140, -175, -250, -325, -400$ and -500 . When dimensionalized by the scale factor ωL , these represent offshore gradient winds ranging from approximately 1 to 10 m sec $^{-1}$. By the symmetry of the problem, the results apply to onshore basic currents if the phase is shifted by π and the land-sea relationship is reversed. In the presence of the basic current, the horizontal velocity will be given by the vector sum of the perturbation and the basic current.

Fig. 6, which shows the u fields at 4-hr intervals, illustrates several effects of the basic current. In addition to the expected offshore advection of the maximum perturbation, there is a considerable smoothing of the peaks of the $u(x)$ curves as $-U_{nd}$ increases. The maximum u at $t=8$ hr decreases from 250 cm sec $^{-1}$ with $U_{nd}=-100$ to 75 cm sec $^{-1}$ with $U_{nd}=-400$. Since the momentum of the disturbance becomes less concentrated in the horizontal as the gradient wind speed increases, we may conclude that the omission of horizontal advection is responsible for the unrealistically large magnitudes of $\partial u/\partial x$ and $\partial w/\partial x$ in the symmetric ($U=0$) case.

The asymmetry in Fig. 6 is such that $|\partial u/\partial x|$ is larger on the landward than on the seaward side of the perturbation maximum. As required by mass continuity, the upward motion is stronger and more concentrated than the offshore downward motion. Maximum vertical velocities corresponding to Fig. 6a are approximately 7 cm sec $^{-1}$ in the updraft and -3 cm sec $^{-1}$ in the offshore subsidence region. This wind pattern is suggestive of the sea breeze front, which has been observed when



the gradient wind is offshore. Although it has been reproduced in the nonlinear numerical models of Estoque (1962) and McPherson (1968), the sea breeze front has not been detected in previous analytic results. The asymmetry in Fig. 6 may be the closest reproduction of a sea breeze front that the linear model will allow, since the periodic time dependence at each point restricts the inland movement of the model's "front."

The asymmetric circulation was found to show the same qualitative dependence of f and N^2 as the symmetric circulation of Section 3a, although these results are not included here.

4. Heat flux calculations

a. Formulation

The mechanism by which the sea breeze generates kinetic energy is the rising of warm air and the sinking of cool air. The net upward heat flux is therefore a measure of the kinetic energy generated by the circulation. By comparing the fluxes associated with the sea breeze and other atmospheric circulations, one can assess the importance of the sea breeze as a feature of the general circulation.

In the notation of Section 2, the time-averaged vertical heat flux along a unit distance of coastline is given by

$$F = (2\pi)^{-1} \int_0^{2\pi} dt \int_{-\infty}^{\infty} \rho c_p w T' dx, \quad (12)$$

where $T' = T_0 - (g/c_p)z$. Using the definition $b = gT'/T_0$, assuming constant ρ , c_p and T_0 , and evaluating the time integrals using (7), one obtains

$$F = \rho c_p T_0 (2g)^{-1} \times \int_{-\infty}^{\infty} (w_{t=0} b_{t=0} + w_{t=\pi/2} b_{t=\pi/2}) dx, \quad U \neq 0, \quad (13a)$$

$$F = \rho c_p T_0 g^{-1} \times \int_0^{\infty} (w_{t=0} b_{t=0} + w_{t=\pi/2} b_{t=\pi/2}) dx, \quad U = 0. \quad (13b)$$

In cgs units, $\rho c_p T_0 g^{-1} \approx 3.0 \times 10^8 \text{ gm cm}^{-2}$.

The flux was evaluated at five values of z for the case of $U = 0$, $f/\omega = 1.5$, $N^2 = 10^{-4} \text{ sec}^{-2}$, and $\kappa = 5 \times 10^4 \text{ cm}^2 \text{ sec}^{-1}$. The results are shown in Fig. 7 as functions of x , which has replaced the upper integration limit in (13b). Convergence is rapid at small z and only slightly slower at large z , indicating that the vertical heat flux decreases rapidly with distance from the coastline. The horizontally integrated flux reaches its maximum value

FIG. 6. The x dependence of the u component of velocity at $z = 0.33$ for the case of $f/\omega = 1.5$, $N^2 = 10^{-4} \text{ sec}^{-2}$, and (a) $U(\omega L)^{-1} = -100$, (b) $U(\omega L)^{-1} = -250$, (c) $U(\omega L)^{-1} = -400$. Otherwise as in legend to Fig. 3.

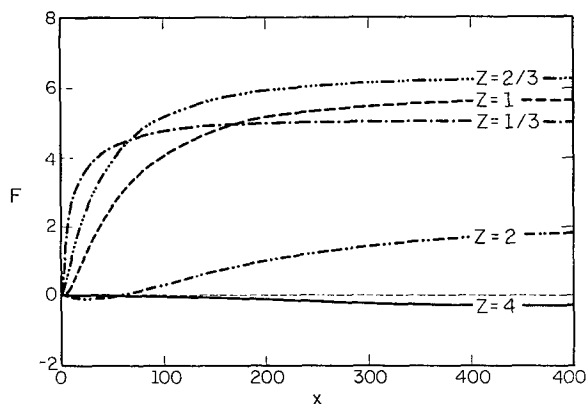


FIG. 7. The time-averaged vertical heat flux [kJ sec⁻¹ cm⁻¹]

$$F(x) = \rho c_p T_0 (2\pi g)^{-1} \int_0^{2\pi} dt \int_{-x}^x w b dx$$

for the case of $f/\omega = 1.5$, $N^2 = 10^{-4} \text{ sec}^{-2}$, $U = 0$. The coordinates x and z are nondimensional; w and b are scaled using $b_{\text{max}} = 9.8 \text{ cm sec}^{-2}$. The integrals are based on the value of $\kappa = 5 \times 10^4 \text{ cm}^2 \text{ sec}^{-1}$.

near $z = 0.67$, several hundred meters above the surface. It is interesting to note that the flux at $z = 4$ is slightly negative, implying that the region above $z = 4$ is forced mechanically by the motion below it. The sea breeze (with $U = 0$) can therefore be said to be confined to $0 \leq z \leq 4$, or approximately the lowest kilometer. If all z are considered, the volume integral of the flux is clearly positive, as it must be if there is to be a net conversion of potential to kinetic energy to offset frictional dissipation.

Since the latitude dependence of the circulation is significant only at large x and z where the velocities are small, the heat flux varies only slightly with f . However, the heat flux depends strongly on the stability. Fig. 8 shows the horizontally integrated flux for two examples of uniform stability and two examples of simulated inversions. (An inversion is simulated with a two-layer model in which N^2 is discontinuous at the interface; at the interface, one must require the continuity of u , v , w , p , b , $\partial u/\partial z$, $\partial v/\partial z$, $\partial w/\partial z$ and $\partial b/\partial z$.) According to Fig. 8, the flux in a case of uniform stability is approximately tripled when N^2 is increased by an order of magnitude. The damping effect of the inversion is apparent in each two-layer case, and the flux maximum is shifted upward or downward into the less stable layer.

The effect of a basic current is illustrated in Fig. 9. The basic current reduces the heat flux and displaces its maximum to a slightly larger value of z . The reduction of the flux is due in part to the small offshore values of b which result from the opposing effects of vertical diffusion and horizontal advection. Since $U_{\text{nd}} = 500$ corresponds to a basic current of $\sim 16 \text{ kt}$, we see that typical gradient winds will reduce the vertical heat flux by approximately a factor of 2.

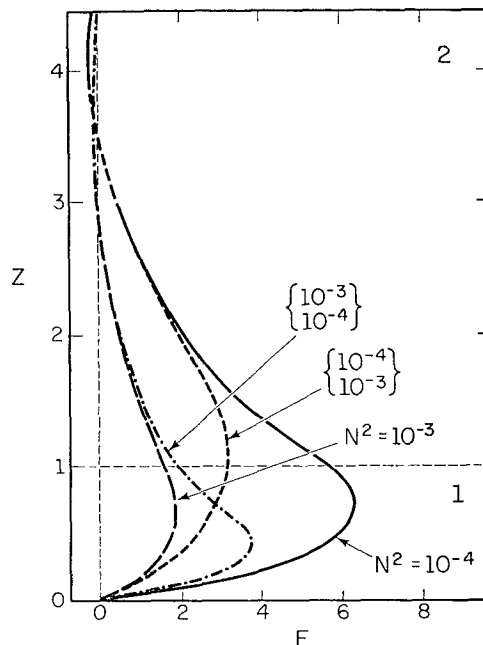


FIG. 8. The horizontally integrated, time-averaged vertical heat flux F (kJ sec⁻¹ cm⁻¹) for four arrangements of N^2 (sec⁻²) with $f/\omega = 1.5$, $U = 0$, $\kappa = 5 \times 10^4 \text{ cm}^2 \text{ sec}^{-1}$. The coordinate z is nondimensional; w and b are scaled using $b_{\text{max}} = 9.8 \text{ cm sec}^{-2}$.

The horizontally integrated flux will also depend on the value of $\kappa^{1/2}$ because x is scaled by the viscous length $L = (\kappa/\omega)^{1/2}$.

b. Application to actual coastal configurations

The model results were used to compute the climatologically averaged vertical heat fluxes due to the sea breeze effect. The coastlines were represented by linear segments, each of which was assigned a value of $(\Delta T)_{\text{max}}$ based on the mean monthly ocean temperature and monthly means of the maximum and minimum land

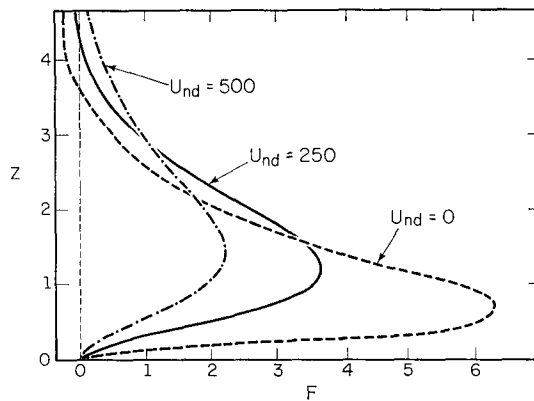


FIG. 9. The horizontally integrated, time-averaged vertical heat flux F (kJ sec⁻¹ cm⁻¹) for three cases in which $f/\omega = 1.5$, $N^2 = 10^{-4} \text{ sec}^{-2}$, $\kappa = 5 \times 10^4 \text{ cm}^2 \text{ sec}^{-1}$. Otherwise as in legend to Fig. 8.

TABLE 2. Computed vertical heat fluxes due to the sea breeze effect (units: 10^{14} J sec $^{-1}$).

	March	June	Sep- tember	De- cember	Annual average
Africa	0.53	0.52	0.58	0.42	0.51
Asia	0.50	0.92	0.60	0.17	0.55
Australia	0.24	0.07	0.24	0.29	0.21
Europe	0.09	0.50	0.23	0.00	0.20
N. America	0.23	0.67	0.33	0.06	0.32
S. America	0.36	0.18	0.39	0.34	0.32
Northern Hemisphere	1.18	2.45	1.45	0.39	1.37 (65%)
Southern Hemisphere	0.76	0.46	0.91	0.89	0.74 (35%)
Total	1.94	2.87	2.36	1.28	2.11

temperatures. The land and sea breeze fluxes were computed separately, and the algorithm reduced the land breeze flux by requiring that it never exceed the sea breeze flux. Since the linear coastal segments were ~ 50 km in length, it was necessary to neglect smaller inlets, peninsulas and islands. Large islands and inland bodies of water (e.g., the Great Lakes) were included. Representation of the coastline by linear segments also removed much of the curvature, although the effects of concavity and convexity should tend to cancel when many segments are included. Stability and the synoptic-scale winds were included only as mean effects: the flux estimates were based on the curve in Fig. 9 for which $N^2 = 10^{-4}$ sec $^{-2}$ and $U_{na} = 250$. Thus, a normal gradient wind component of ~ 8 kt was used to represent the averaged influence of synoptic circulations. The $\kappa^{\frac{1}{2}}$ dependence of the flux was unchanged by the summation over y because the coastal lengths are dimensional; the flux estimates are based on $\kappa = 5 \times 10^4$ cm 2 sec $^{-1}$.

Because of the sinusoidal time dependence of the forcing function, the results of the model are applicable only to the equinoctial months (March, September). However, calculations were also made for the months of June and September in order to gain a crude estimate of the summer and winter heat fluxes. At the summer solstice, the theoretical calculations will underestimate the sea breeze flux and overestimate the land breeze flux. At the winter solstice, the reverse is true.

The computed fluxes are presented in Table 2. The values are for $z \approx 1$, where the flux reaches its maximum value according to Fig. 9. The continents of Asia and Africa contribute the largest amounts to the total flux. While Africa's equatorial location results in little seasonal variation, Asia's more northerly location leads to a strong seasonal dependence. The Asian value for June (the monsoon season) is larger than any other monthly flux value. Europe and North America also show the expected strong seasonal dependence. The fact that the Northern Hemisphere contains most of the world's land mass is reflected in the results, which show that 65% of the heat flux occurs in the Northern Hemisphere. The northern summer month of June contributes the

most to the annual total, while the southern summer month of December contributes the least.

c. Significance of the heat flux estimates

In the middle and upper troposphere, synoptic-scale eddies and the mean meridional cells accomplish most of the upward transport of sensible heat. Small-scale eddies, referred to as convective turbulence, dominate the transport in the lower troposphere. The cloud patterns which appear in satellite photographs suggest that the sea breeze effect plays a role in organizing convective turbulence (Bugaev, 1973). The importance of this role is indicated by the relative magnitudes of the sea breeze and total vertical heat fluxes. Unfortunately, the magnitude of the total vertical flux of sensible heat is uncertain because it cannot be measured directly. In studies of the atmosphere's heat budget, the sensible heat flux is generally assigned the value required to balance the net effect of the other thermal processes. It therefore includes the sum of the errors in the estimates of all the other quantities. These errors are reflected in the variability of the previous estimates of the total vertical flux of sensible heat:

Kondratyev (1969)	6.8×10^{15} J sec $^{-1}$
Budyko (1958)	8.5×10^{15} J sec $^{-1}$
London (1957)	19.0×10^{15} J sec $^{-1}$
Houghton (1954)	17.3×10^{15} J sec $^{-1}$

Although these values are for the surface, they probably do not vary significantly in the lowest kilometer. The four estimates of the total sensible heat flux are to be compared with the annual average of the sea breeze heat flux (2.1×10^{14} J sec $^{-1}$) as estimated in Section 4b. Since the four previous estimates agree on the order of magnitude of the total flux, and since the sea breeze flux is computed from realistic values of w and b , one may conclude that the sea breeze effect accounts for between 1 and 3% of the vertical flux of sensible heat at a height of several hundred meters. Above and below the level where the sea breeze flux reaches its maximum value, the percentage is smaller.

A comparison can also be made with the upward heat transport accomplished by an extratropical cyclone. For the synoptic case of 4–5 April 1950, Palmèn and Newton (1969) calculate a heat flux of 2.3×10^{14} J sec $^{-1}$ at 500 mb, the approximate level at which synoptic-scale transports reach their maximum values. Therefore, in terms of the vertical transport of sensible heat, the globally integrated effect of the sea breeze at $z \approx 250$ m is comparable to the effect at 500 mb of one extratropical cyclone.

5. Application to the sea breeze prediction problem

The scaling of the velocity components by b_{\max}/ω enables one to determine the land-sea temperature difference that is necessary to create a positive $u_{\text{total}} = u$

+ U at any point for a specified offshore U . Alternatively, for a given $(\Delta T)_{\max}$, one can determine the magnitude of the offshore gradient wind that is necessary to prevent a net onshore flow. Such a relationship between U and ΔT is of practical importance in forecasting the occurrence of a sea breeze or a lake breeze.

Empirical relations have been developed from observations made at various coastal stations. Biggs and Graves (1962) and Lyons (1972), for example, use the following relation to forecast lake breeze occurrences on the western shores of Lakes Erie and Michigan:

$$(\Delta T)_{\max} > \epsilon V_i^2,$$

where V_i is the average surface wind speed (m sec^{-1}) irrespective of direction at an inland site and $(\Delta T)_{\max}$ is the maximum land-water temperature difference ($^{\circ}\text{C}$); ϵ is an empirically determined constant, the value of which is $\frac{1}{3}\text{C m}^{-2}\text{sec}^{-2}$ according to Biggs and Graves. For comparison to the results of the linear model, we assume $V_i = 2^{1/2}V_{\text{in}}$ to obtain an average component V_{in} normal to the coast. The empirical relation is then

$$(\Delta T)_{\max} > 2\epsilon V_{\text{in}}^2. \tag{14}$$

In the notation of the model, where $b_{\max} = g(\Delta T)_{\max}/(2T_0)$ and $V_{\text{in}} = U$, this empirical criterion becomes

$$\frac{b_{\max}}{\omega^2 L} > \frac{g}{T_0} \left(\frac{\kappa}{\omega}\right)^{3/2} \left(\frac{U}{\omega L}\right)^2. \tag{15}$$

The scaling of Section 2 enables the theoretical criterion $(u+U)_{x=0} > 0$ to be written as

$$\frac{b_{\max}}{\omega^2 L} > \frac{1}{\max} \frac{|U|}{\omega L}, \tag{16}$$

where $u_{\max}(f/\omega, N^2/\omega^2, U/\omega L)$ is the maximum (non-dimensional) value of u obtained in the solution. We ignore the functional dependence of u_{\max} on f/ω and N^2/ω^2 because the observational data do not allow such dependence.

Although the sea breeze occurrence criteria are defined for the coastline, (16) will be interpreted using the maximum value of u even if it occurs offshore. This choice of u_{\max} anticipates the nonlinear self-advection of the disturbance. Tests in Section 6 verify the intuitive idea that self-advection does displace u_{\max} back to the coastline.

By equating the right sides of (15) and (16), one obtains

$$\frac{u_{\max}}{\omega L} \frac{|U|}{\omega L} = \frac{1}{\epsilon} \frac{T_0}{g} \left(\frac{\omega}{\kappa}\right)^{3/2} = C, \tag{17}$$

where C is a constant. Thus, if (15) and (16) are equivalent, the product of the nondimensional quantities u_{\max} and $|U|/(\omega L)$ should be a constant independent of the value of the basic current. Fig. 10 shows that

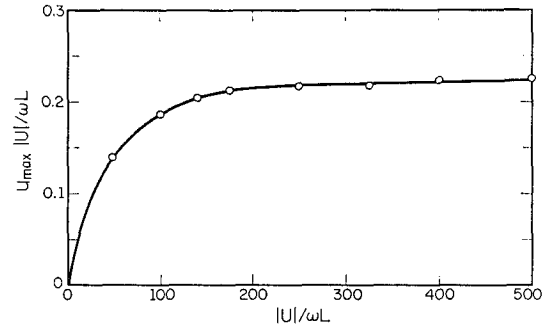


FIG. 10. The product $u_{\max}|U|/(\omega L)$ as a function of $|U|/(\omega L)$: $f/\omega = 1.5$, $N^2 = 10^{-4}\text{sec}^{-2}$.

$u_{\max}|U|/(\omega L)$ is indeed nearly constant except at small $|U|$, where the vanishing of $|U|$ requires that the product also vanish. One may now use (17) and the asymptotic value of $C = 0.22$ to replace ϵ by an expression which can be interpreted physically:

$$\epsilon = \frac{T_0}{0.22g} \left(\frac{\omega}{\kappa}\right)^{3/2}.$$

The original empirical criterion (14) can then be written as

$$(\Delta T)_{\max} > 2\epsilon U^2 = \frac{T_0}{0.11g} \left(\frac{\omega}{\kappa}\right)^{3/2} U^2. \tag{18}$$

According to (18), ϵ and the critical $(\Delta T)_{\max}$ increase as the forcing frequency increases. Physically, a rapidly oscillating forcing function implies that there is little time for the circulation to increase in intensity by the potential \rightarrow kinetic energy conversion. Therefore, if a critical perturbation velocity is to develop, there must be a large amount of available potential energy, or a large $(\Delta T)_{\max}$. Eq. (18) also implies that an increase in the eddy conduction coefficient κ decreases ϵ and the critical $(\Delta T)_{\max}$. This result is consistent with the fact that conduction is the process which creates available potential energy for the sea breeze circulation.

When the computed value of C [$=0.22$] and the value of ϵ based on the Biggs and Graves data are substituted into (17), the diffusion coefficient most appropriate to the daytime phase of the lake breeze can be evaluated. The result, $\kappa = 1.1 \times 10^5 \text{cm}^2 \text{sec}^{-1}$, agrees well with the daytime eddy diffusivity of $10^5 \text{cm}^2 \text{sec}^{-1}$ used by Kuo (1968) and Yoshikado and Asai (1972). The mean value of $\kappa = 5 \times 10^4 \text{cm}^2 \text{sec}^{-1}$ used to scale L and U in the model calculations is probably a reasonable compromise between the daytime value of $10^5 \text{cm}^2 \text{sec}^{-1}$ and the nighttime value, which is likely to be at least an order of magnitude smaller than the daytime value.

The theoretical criterion based on $\kappa = 10^5 \text{cm}^2 \text{sec}^{-1}$ is compared with the empirical criterion in Fig. 11. Sea breeze occurrence by the theoretical criterion requires a

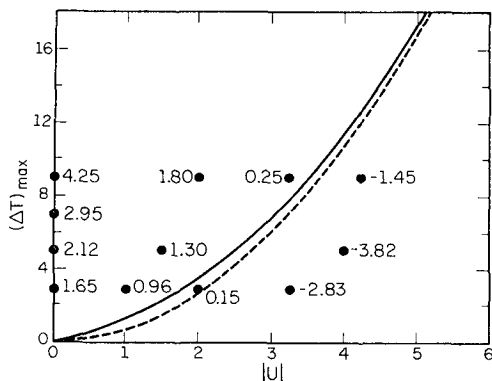


FIG. 11. The critical land-sea temperature difference (ΔT)_{max} required for sea breeze occurrence. U (m sec⁻¹) is scaled using $\kappa = 10^5$ cm² sec⁻¹. Solid curve is the linear criterion (see text), dashed curve is based on the observational data of Biggs and Graves (1962). Numbers accompanying circles are the values of $(U+u)$ _{max} in the region $x \geq 0$ based on the nonlinear integrations of Section 6; positive values indicate sea breeze occurrence.

slightly larger $(\Delta T)_{\max}$ for $|U| \leq 6$ m sec⁻¹ and a slightly smaller $(\Delta T)_{\max}$ for $|U| \geq 6$ m sec⁻¹, although the latter portion of the curve is not shown because both criteria require such large values of $(\Delta T)_{\max}$ for $|U| \geq 6$ m sec⁻¹ that sea breezes will rarely occur. For all $|U| \leq 10$ m sec⁻¹, the curves agree to within 1C. It is to be noted that the use of a mean κ based on observational data assures only a "mean" agreement between the theoretical and empirical curves over the range $|U| \leq 10$ m sec⁻¹. Such a value of κ does not guarantee that the curves will agree as closely as they do at each value of U . One may therefore conclude that the model provides theoretical support for the observed linear relationship between U^2 and the critical $(\Delta T)_{\max}$.

6. The nonlinear model

The results in Section 3 show that the linear model can describe many of the observed features of the sea breeze. There remains the task of examining the nonlinear advection process, the omission of which appears to be the most serious shortcoming of the linear model. The effect of nonlinear momentum advection was already anticipated in Section 5, where a criterion for sea breeze occurrence was based on the assumption that the maximum perturbation velocity will be found at the coastline.

As noted in Section 1, a finite-difference mesh must be fine enough to resolve the steep temperature and velocity gradients near the coastline. Yet the domain must be large enough to avoid contamination to the solution by the artificial lateral boundaries. In view of the stability problems encountered in earlier models based on coordinate stretching, this study will use the "overlapping grid" technique to achieve the desired resolution near $x = 0$. This technique, which may have applications in the study of other mesoscale phenomena,

has the advantage that the time step may be increased in regions far from the coastline. The grid network is described in the Appendix.

The system to be integrated is the hydrostatic version of (1)-(5) with the nonlinear advection terms included in flux form:

$$\left. \begin{aligned} \frac{\partial u}{\partial t} + \frac{\partial}{\partial x}(Uu+u^2) + \frac{\partial}{\partial z}(wu) - fv &= -\frac{\partial p}{\partial x} + \nu \frac{\partial^2 u}{\partial z^2} \\ \frac{\partial v}{\partial t} + \frac{\partial}{\partial x}(Uv+uv) + \frac{\partial}{\partial z}(wv) + fu &= \nu \frac{\partial^2 v}{\partial z^2} \\ \frac{\partial b}{\partial t} + \frac{\partial}{\partial x}(Ub+ub) + \frac{\partial}{\partial z}(wb) + N^2 w &= \kappa \frac{\partial^2 b}{\partial z^2} \\ b &= \frac{\partial p}{\partial z} \\ \frac{\partial u}{\partial x} + \frac{\partial w}{\partial z} &= 0 \end{aligned} \right\} \quad (19)$$

The finite difference form of (19) as well as the boundary conditions are contained in the Appendix.

Table 3 summarizes the integrations which were performed with the finite-difference model. In each case, the external parameters were $f/\omega = 1.5$, $N^2 = 10^{-4}$ sec⁻², $\nu = \kappa = 5 \times 10^4$ cm² sec⁻¹. The integrations were carried out to $t = 8$ hr, at which time the maximum wind speeds have just begun to decrease. The weakening stage of the sea breeze was not examined because it does not aid in the formulation of a sea breeze occurrence criterion.

When no basic current is present, the perturbations show the expected onshore movement. Fig. 12 shows the isopleths of u and b at $t = 8$ hr for the case of $(\Delta T)_{\max} = 3C$, $U = 0$. Even though the circulation is

TABLE 3. Summary of the nonlinear numerical integrations. "Levels" refers to the number of grid points in the vertical; u_{\max} is the maximum value of u at $t = 8$ hr. The final column gives the x coordinate of the grid point at which u_{\max} occurs.

Run no.	Levels	$(\Delta T)_{\max}$ (°C)	$-U$ (m sec ⁻¹)	u_{\max} (m sec ⁻¹)	x coordinate (km)
1a	10	3C	0.0	1.65	2.75
1b	10	3C	1.0	1.96	1.75
1c	20	3C	2.0	2.15	0.75
1d	20	3C	3.25	1.13	-4.25
2a	10	5C	0.0	2.12	4.75
2b	20	5C	1.5	2.80	1.75
2c	20	5C	4.0	1.48	-4.25
3	10	7C	0.0	2.95	6.50
4a	10	9C	0.0	4.75	9.25
4b	20	9C	2.0	3.80	4.25
4c	20	9C	3.25	3.50	0.25
4d	20	9C	4.25	3.10	-3.00
5*	10	5C	1.5	2.44	-3.00

* In Run 5, the nonlinear advection terms were omitted.

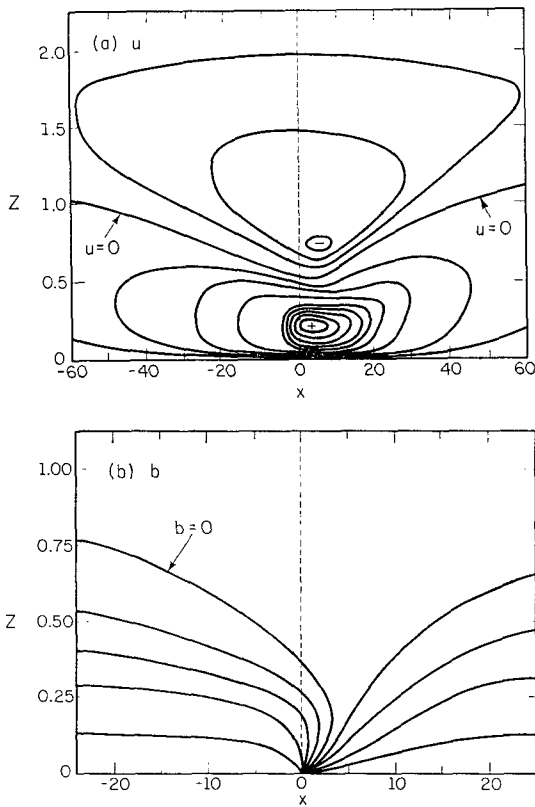


FIG. 12. Isopleths of u (0.2 m sec^{-1} intervals) and b (0.1 m sec^{-1} intervals) at $t=8 \text{ hr}$ for the nonlinear case in which $(\Delta T)_{\text{max}}=3C$, $U=0$, $f/\omega=1.5$, $N^2=10^{-4} \text{ sec}^{-2}$. The coordinates x and z are in kilometers.

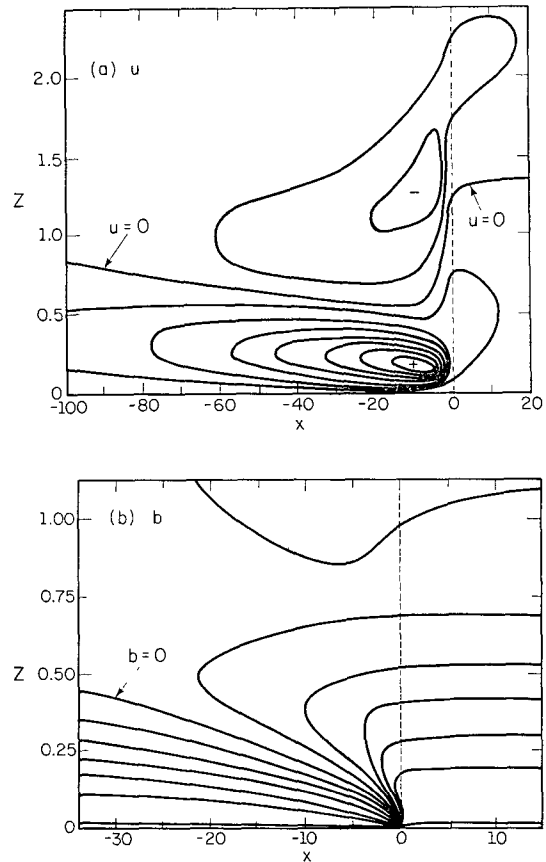


FIG. 13. As in Fig. 12 except for $(\Delta T)_{\text{max}}=5C$, $U=-4.0 \text{ m sec}^{-1}$.

weak, the maximum velocity perturbations have been advected several kilometers inland. Cooler offshore temperatures have also been advected across the coastline, as was anticipated in Section 3. The depth of the onshore flow and the relative intensities of the low-level and return currents are in good agreement with the linear results.

Fig. 13 shows the results for the case of $(\Delta T)_{\text{max}}=5C$, $U=-4 \text{ m sec}^{-1}$. In the presence of the basic current, the perturbation has assumed a frontal character. The steepest gradients are slightly offshore in Fig. 13 because of the strong basic current in this particular case.

The x coordinate of the maximum perturbation is examined as a function of time in Fig. 14. In this example, the basic current is of approximately the same magnitude as the maximum perturbation velocity. The nonlinear model predicts that u_{max} will be advected offshore during the early part of the day. Then, as the circulation becomes stronger, u_{max} moves back toward the coast. Fig. 14 which contrasts the behavior of the nonlinear and linear models, supports the assumption of Section 5 that u_{max} will be found at the coastline when $u_{\text{max}} \approx |U|$.

Fig. 15 shows the effect of nonlinear advection of u_{max} when the basic current is strong. In this case, the per-

turbation is not strong enough to advect u_{max} back to the coastline, but it is clearly able to retard the offshore advection. $|U|$ is large enough that Fig. 15 represents a non-sea-breeze case by either criterion of Fig. 11.

The validity of the nonlinear model as a sea breeze predictor is seen in Fig. 11, which locates runs 1a-5 in U , $(\Delta T)_{\text{max}}$ space. Each point is marked with the maxi-

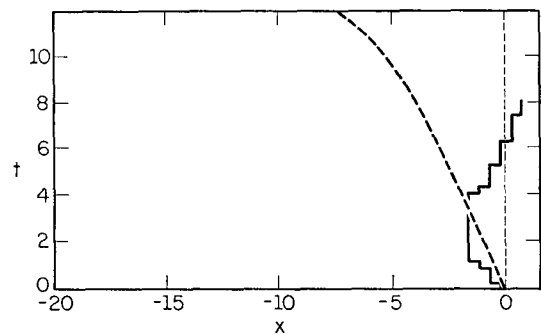


FIG. 14. The x coordinate of the maximum value of u as a function of time (hours after sunrise). Solid curve shows u_{max} at $k=1$ ($z=125 \text{ m}$) for the nonlinear case: $(\Delta T)_{\text{max}}=3C$, $U=-2.0 \text{ m sec}^{-1}$. Dashed curve shows u_{max} at $z=0.33$ ($\sim 100 \text{ m}$) for the linear case: $(\Delta T)_{\text{max}}=3C$, $U=-1.8 \text{ m sec}^{-1}$. In each case, $\nu=\kappa=5 \times 10^4 \text{ cm}^2 \text{ sec}^{-1}$.

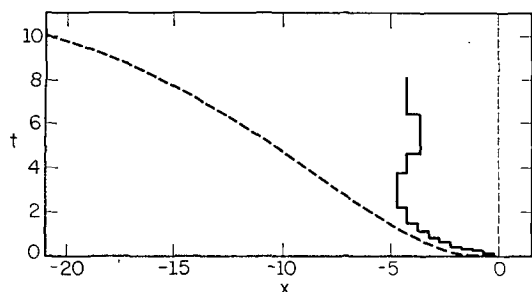


FIG. 15. As in Fig. 14 except for $(\Delta T)_{\max} = 5C$, $U = -4.0$ m sec $^{-1}$ (solid curve) and $(\Delta T)_{\max} = 5C$, $U = -4.5$ m sec $^{-1}$ (dashed curve).

imum value of $(U+u)$ which occurs in the region $x \geq 0$ at $t = 8$ hr. Since positive values imply that a sea breeze exists over land, the nonlinear results are quite consistent with the empirical criterion. The nonlinear results also agree well with the linear criterion described in Section 5.

When the land-sea temperature difference is made larger than about 9C, numerical instabilities begin to appear in the nonlinear results. Significantly, the instabilities develop not in a region of grid overlap, but in the central grid where $|\partial u/\partial x|$ and $|\partial w/\partial x|$ are largest. As these large values of $|\partial(u,w)/\partial x|$ move inland with the sea breeze front, the most severe numerical instabilities also move inland. A tentative hypothesis is that the instabilities reflect the inability of (19) to handle the behavior of the nonlinear system in a region where nonhydrostatic effects may be significant.

7. Summary and conclusions

This study has explored the capabilities and limitations of several simple sea breeze models. The symmetric ($U=0$) linear circulation's most realistic feature, which was shown to be due to the neglect of advection, is the concentration of large velocities near the coastline. When advection by a basic current ($U \neq 0$) is included, the velocities near the coastline are reduced considerably. The asymmetry in the velocity field when $U \neq 0$ is suggestive of a tendency toward the formation of a sea breeze front.

The dependence of the linear circulation on the external parameters has been explored with an eye toward several applications of the results. In one application, heat flux calculations indicated that the sea breeze component of the general circulation can account for several percent of the total vertical flux of sensible heat at a height of several hundred meters.

The results have provided theoretical support for the empirical sea breeze occurrence criterion $(\Delta T)_{\max} > \epsilon U^2$, and a physical interpretation of the parameter ϵ has been obtained. The vertical variation of U , which was not considered here, could be included in a multi-layer model similar to that used in the inversion simulation which was mentioned in Section 4.

The nonlinear "self-advection" of the sea breeze was found to account for a landward displacement of the velocity maximum. The displacement of several kilometers was anticipated when the linear results were applied to the sea breeze prediction problem. The overlapping grid technique, which was used to examine the nonlinear advection process, appears to be both feasible and useful in the study of mesoscale circulations. The application of this technique in smaller scale problems may be possible if the hydrostatic assumption is abandoned.

Acknowledgments. The author wishes to thank Dr. Norman Phillips for serving as thesis advisor during the course of this work. Funding was provided in part by an NDEA Title IV Fellowship and in part by the National Science Foundation under Grant GA 28724.

APPENDIX

Formulation of the Nonlinear Model

Fig. 16 shows the relative positions of the seven overlapping grids. The vertical space increment is the same for each grid: $\Delta z = H/K$, where H is the height of the lid and K the number of levels. The central grid (4) contains 40 points in the horizontal while each of the other six grids contains 20 points in the horizontal. The horizontal space increments are specified to give finer resolution near the coastline, and the time increments are proportional to Δx :

Grid no.	Δx	Δt
1	4.0 km	240 sec
2	2.0 km	120 sec
3	1.0 km	60 sec
4	0.5 km	30 sec

This arrangement of grid points requires less than one-third the core storage and less than one-sixth the computing time of a uniform fine mesh, $\Delta x \leq 0.5$ km, covering the same area. A model based on coordinate stretching requires an intermediate amount of computing time because the uniform value of Δt must correspond to the smallest value of Δx .

At the boundaries of adjacent grids, the "two-way" interaction scheme of Phillips and Shukla (1973) is used. The forecasts for the coarse and fine grids are made independently, but the innermost column of the coarse grid and the outermost two columns of the fine grid are interpolated from the other grid. Linear interpola-

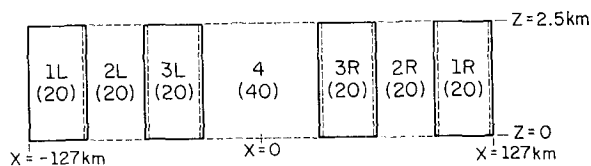


FIG. 16. Relative positions of the seven overlapping grids. L and R denote the left and right portions, respectively. Values in parentheses indicate the number of grid points in the horizontal.

tion formulas are used. The overlap is designed to be as small as possible without requiring interpolation between values which have themselves been interpolated. Any "noise" resulting from the interaction at the grid boundaries is minimized by using a two-step Lax-Wendroff differencing scheme which has been found to be well-behaved computationally, i.e., additional "smoothing" or periodic adjustments are not required to avoid computational instability. The differencing scheme is based on the time- and space-staggered lattice suggested by Eliassen [(1956); see also Phillips (1962)]. The spatial arrangement of the variables is shown in Fig. 17, where j and k are the horizontal and vertical indices, respectively. An "uncentered difference," upstream trajectory computation is used to evaluate the "prime" quantities u', v', b' at the half-timestep. A centered difference formulation of the "flux" form of the equations is then used to evaluate u, v, b for the next full-timestep. The full-timestep equations corresponding to (19) are

$$\begin{aligned}
 u_{jk,n+1} &= u_{jk,n} - \sigma_x (FXU_{jk} - FXU_{j-1k}) - (\sigma_z/4) \\
 &\quad \times (FZU_{jk+1} - FZU_{jk}) - \sigma_x (p'_{jk} - p'_{j-1k}) + \lambda v'_{jk} \\
 &\quad + \delta (u_{jk+1n} - 2u_{jk,n} + u_{jk-1n}), \\
 v_{jk,n+1} &= v_{jk,n} - \sigma_x (FXV_{j+1k} - FXV_{jk}) - (\sigma_z/4) \\
 &\quad \times (FZV_{j+1k+1} + FZV_{jk+1} - FZV_{j+1k} - FZV_{jk}) \\
 &\quad - \lambda u'_{jk} + \delta (v_{jk+1n} - 2v_{jk,n} + v_{jk-1n}), \\
 b_{jk,n+1} &= b_{jk,n} - \sigma_x (FXB_{jk} - FXB_{j-1k}) - (\sigma_z/4) \\
 &\quad \times (FZB_{jk+1} - FZB_{jk}) - (\eta/2) (w'_{jk+1} + w'_{jk}) \\
 &\quad + \delta (b_{jk+1n} - 2b_{jk,n} + b_{jk-1n}), \\
 p_{jk,n} &= p_{j,k-1n} + \Delta z (b_{jk,n} + b_{j,k-1n})/2, \\
 w_{jk+1n} &= w_{jk,n} - (\Delta z/\Delta x) (u_{j+1kn} - u_{jk,n}),
 \end{aligned}$$

where $\sigma_{(x,z)} \equiv \Delta t/\Delta(x,z)$, $\lambda \equiv f\Delta t$, $\eta \equiv N^2\Delta t$ and $\delta \equiv \nu\Delta t/(\Delta z)^2$ ($\nu = \kappa$). The flux terms are given by

$$\left. \begin{aligned}
 FXU_{jk} &\equiv (U + u'_{jk})^2 \\
 FZU_{jk} &\equiv w'_{jk} (u'_{jk} + u'_{j-1k} + u'_{jk-1} + u'_{j-1k-1}) \\
 FXV_{jk} &\equiv v'_{jk} [U + (u'_{jk} + u'_{j-1k})/2] \\
 FZV_{jk} &\equiv w'_{jk} (v'_{jk} + v'_{j,k-1}) \\
 FXB_{jk} &\equiv b'_{jk} (U + u'_{jk}) \\
 FZB_{jk} &\equiv w'_{jk} (b'_{jk} + b'_{j-1k} + b'_{jk-1} + b'_{j-1k-1})
 \end{aligned} \right\}$$

The half-timestep (prime) variables have previously been computed from the equations

$$\begin{aligned}
 u'_{jk} &= u^*_{jk,n} - (\sigma_x/2) (p_{j+1k} - p_{jk}) + (\lambda/2) v_{jk,n} + (\delta/4) \\
 &\quad \times [(u_{j+1} + u_j)_{k+1n} - 2(u_{j+1} + u_j)_{kn} \\
 &\quad + (u_{j+1} + u_j)_{k-1n}], \\
 v'_{jk} &= v^*_{jk,n} - (\lambda/2) u_{jk,n} + (\delta/4) [(v_j + v_{j+1})_{k+1n} \\
 &\quad - 2(v_j + v_{j-1})_{kn} + (v_j + v_{j-1})_{k-1n}], \\
 b'_{jk} &= b^*_{jk,n} - (\eta/2) (w_{jk+1n} + w_{jk,n}) + (\delta/4) [(b_{j+1} + b_j)_{k+1n} \\
 &\quad - 2(b_{j+1} + b_j)_{kn} + (b_{j+1} + b_j)_{k-1n}], \\
 p'_{jk} &= p'_{jk-1} + \Delta z (b'_{jk} + b'_{jk-1})/2, \\
 w'_{jk+1} &= w'_{jk} - (\Delta z/\Delta x) (u'_{jk,n} - u'_{j-1kn}).
 \end{aligned}$$

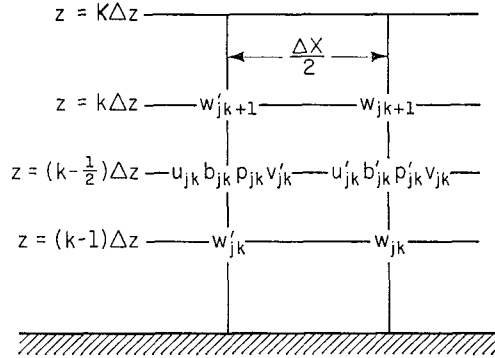


FIG. 17. The modified version of the Eliassen finite-difference grid.

Asterisks denote the values of u, v, b at $t = n\Delta t$ at the point upstream the distance $(-\bar{u}\Delta t/2, -\bar{v}\Delta t/2)$ from the point corresponding to the location of u', v', b' at the half-timestep. Overbars represent averages of the nearest surrounding values of u, v, b . Values of u^*, v^*, b^* are interpolated bilinearly from the four surrounding points of u, v, b , respectively. Two of these points are at the same level as u', v', b' , while the other two are located above or below depending on the sign of \bar{w} .

The lower boundary conditions are the same as in the linear model except for the removal of the discontinuity in the forcing function: b_0 is halved at the two grid points surrounding $x=0$. All perturbations are assumed to vanish at $z=H=2.5$ km, a height at which the linear model predicts very small ($\lesssim 10$ cm sec⁻¹) velocities. At the extreme lateral boundaries, periodicity is assumed if $U=0$. If $U \neq 0$, the x derivatives of all the perturbations are assumed to vanish at the outflow boundary, while at the inflow boundary the velocity perturbations are assumed to vanish and b is forecast using only vertical diffusion. Unlike the linear model, the nonlinear model begins from a state of rest at $t=0$.

REFERENCES

Biggs, W. G., and M. E. Graves, 1962: A lake breeze index. *J. Appl. Meteor.*, **1**, 474-480.
 Budyko, M. I., 1958: *The Heat Balance of the Earth's Surface*. Moscow, Gidrometeor. Translated by the U. S. Weather Bureau, 259 pp.
 Bugaev, V. A., 1973: Dynamic climatology in light of satellite information. *Bull. Amer. Meteor. Soc.*, **54**, 394-418.
 Defant, F., 1951: Local winds. *Compendium of Meteorology*, Boston, Mass., Amer. Meteor. Soc., 655-662.
 Eliassen, A., 1956: A procedure for numerical integration of the primitive equations of the two-parameter model of the atmosphere. Sci. Rept. No. 4, Dept. of Meteorology, University of California at Los Angeles, 53 pp.
 Estoque, M. A., 1961: A theoretical investigation of the sea breeze. *Quart. J. Roy. Meteor. Soc.*, **87**, 136-146.
 —, 1962: The sea breeze as a function of the prevailing synoptic situation. *J. Atmos. Sci.*, **19**, 244-250.
 Fisher, E. L., 1960: An observational study of the sea breeze. *J. Meteor.*, **17**, 645-660.
 —, 1961: A theoretical study of the sea breeze. *J. Meteor.*, **18**, 216-233.

- Geisler, J. E., and F. P. Bretherton, 1969: The sea-breeze fore-runner. *J. Atmos. Sci.*, **26**, 82-95.
- Houghton, H. G., 1954: On the annual heat budget of the Northern Hemisphere. *J. Meteor.*, **11**, 1-9.
- Kondratyev, K. Y., 1969: *Radiation in the Atmosphere*. New York, Academic Press, 912 pp.
- Kuo, K. L., 1968: The thermal interaction between the atmosphere and the earth and the propagation of diurnal temperature waves. *J. Atmos. Sci.*, **25**, 682-705.
- Lettau, H. H., 1949: Isotropic and non-isotropic turbulence in the atmospheric surface layer. AFCRL Geophys. Res. Papers, No. 1, 86 pp.
- , 1951: Theory of surface-temperature and heat-surface oscillations near a level ground surface. *Trans. Amer. Geophys. Union*, **32**, 189-200.
- London, J., 1957: A study of the atmospheric heat balance. Final Report, Project 131, Dept. of Meteor. Oceanogr., New York University.
- Lyons, W. A., 1972: The climatology and prediction of the Chicago lake breeze. *J. Appl. Meteor.*, **11**, 1259-1270.
- Malkus, J. S., and M. E. Stern, 1953: The flow of a stable atmosphere over a heated island, Part I. *J. Meteor.*, **10**, 30-41.
- McPherson, R. D., 1968: A three-dimensional numerical study of the Texas coast sea breeze. Rept. No. 15, College of Engineering, University of Texas, 254 pp.
- Moroz, W. J., 1967: A lake breeze on the eastern shore of Lake Michigan: Observations and model. *J. Atmos. Sci.*, **24**, 337-355.
- Neumann, R. J., and B. A. Mahrer, 1971: A theoretical study of the land and sea breeze circulation. *J. Atmos. Sci.*, **28**, 532-542.
- Ogura, Y., and N. A. Phillips, 1962: Scale analysis of deep and shallow convection in the atmosphere. *J. Atmos. Sci.*, **19**, 173-179.
- Olfe, D. B., and R. L. Lee, 1971: Linearized calculations of urban heat island convection effects. *J. Atmos. Sci.*, **28**, 1374-88.
- Palmén, A., and C. W. Newton, 1969: *Atmospheric Circulation Systems*. New York Academic Press, 603 pp.
- Phillips, N. A., 1962: Numerical integration of the hydrostatic system of equations with a modified version of the Eliassen finite difference grid. *Proc. Intern. Symp. Numerical Weather Prediction*, Tokyo.
- , and J. Shukla, 1973: On the strategy of combining coarse and fine grid meshes in numerical weather prediction. *J. Appl. Meteor.*, **12**, 763-770.
- Pielke, R. A., 1972: Comparison of a hydrostatic and an anelastic dry shallow primitive equation model. NOAA Tech. Memo. ERL OD-13, 47 pp.
- , 1973: A three-dimensional numerical model of the sea breezes over south Florida. NOAA Tech. Memo. ERL-WMPO-2, Weather Modification Program Office, Boulder, Colo., 136 pp.
- Pierson, W. J., Jr., 1950: The effects of eddy viscosity, Coriolis deflection, and temperature fluctuation on the sea breeze as a function of time and height. *Meteor. Papers N. Y. Univ.* **1**, No. 2, 29 pp.
- Schmidt, F. H., 1947: An elementary theory of the land and sea breeze circulation. *J. Meteor.*, **4**, 9-15.
- Smith, R. C., 1955: Air motion over a heated land mass. *Quart. J. Roy. Meteor. Soc.*, **81**, 382-395.
- Tables of Temperature, Relative Humidity, and Precipitation for the World*, 1958: London, British Meteorological Office.
- U. S. Navy, Marine Climatic Atlas of the World*, 1959: NAVAER 50 1C-54, Washington, D. C., Govt. Printing Office.
- Yoshikado, Y., and T. Asai, 1972: A numerical experiment of effects of turbulent transfer processes on the land and sea breeze. *Contrib. Geophys. Inst. Kyoto Univ.*, No. 12, 33-48.